Molecular-dynamics simulations of atomic-scale friction of diamond surfaces

J. A. Harrison,* C. T. White, R. J. Colton, and D. W. Brenner
Chemistry Division, Code 6170, Naval Research Laboratory, Washington, D.C., 20375-5320
(Received 11 May 1992; revised manuscript received 6 August 1992)

The friction which occurs when two diamond (111) hydrogen-terminated surfaces are placed in sliding contact is investigated for sliding in different crystallographic directions, as a function of applied load, temperature, and sliding velocity. We find a directional dependence to the friction coefficient, μ; that for certain crystallographic sliding directions μ increases with increasing load and as the temperature decreases; and that for the sliding speeds investigated here, μ is approximately independent of sliding velocity. We also found that the sliding velocity may become a factor for very slow, experimentally achievable sliding velocities when sliding in the $[11\bar{2}]$ direction but not for sliding in the $[1\bar{1}0]$ direction.

I. INTRODUCTION

Recent advances in the chemical vapor deposition of diamond films hold promise for producing hard protective coatings on a variety of substrates. As a result, it has become important to understand the friction and wear properties of diamond coatings. While a number of studies of the macroscopic tribiological properties of diamond and diamond films[1-8] exist, relatively little is known about the mechanism of diamond friction and wear at the atomic scale.

Current technology has brought us to the point where we can begin to investigate atomic-scale processes at sliding interfaces. Experimentally, the use of the atomic force microscope (AFM) has led to the observation of a frictional force resolved on the atomic scale.[9,10] Theoretically, friction that arises from slippage at solid-solid interfaces has been investigated using molecular dynamics[11] (MD) and first-principles calculations.[12,13] The interactions that occur at a tip-surface sliding interface (analogous to an AFM experiment) have also been investigated using molecular dynamics.[14]

There are also several early models, specifically developed to examine the mechanism of energy dissipation, which have been used to examine the wearless friction that occurs when two atomically flat surfaces are placed into sliding contact.[15,16] These models agree qualitatively with one another and with molecular-dynamics simulations of friction between close-packed films.[17] The phenomenon of wearless friction has also been examined by Sokoloff[13,18] and by Hirano and Shinjo.[19]

In this work, we use molecular dynamics to investigate atomic-scale friction and associated processes between two atomically flat diamond surfaces in sliding contact. The simulations employed here allow for a detailed examination of the friction phenomenon. In particular, we have examined atomistic sliding and energy dissipation mechanisms; the dependence of the friction coefficient on crystallographic sliding direction, temperature, and load; and the effect of sliding speed on the friction process. We also briefly compare our detailed results with earlier models of wearless friction.

II. METHODOLOGY

The MD calculations are carried out by integrating Newton's equations of motion with a third-order Nordsieck predictor corrector[20] using a constant time step of 0.5 fs. The forces are derived from an empirical hydrocarbon potential that is capable of modeling intramolecular chemical bonding in both diamond and graphite lattices, as well as in a variety of small hydrocarbon molecules.[21-25] The potential used here is potential II of Ref. 22 with additional terms that better describe torsional forces[23] and short-range, repulsive terms[21] that may prove important under high compression. (Although it was not a factor in this work, this potential allows for the modeling of chemical reactivity, unlike more traditional valence-force fields. The importance of this capability in friction studies will be demonstrated in subsequent publications.) Recently, this potential has been used to model the compression of C_{60} between graphite planes,[23] the scattering of C_{60} from diamond surfaces,[24] and the compression and indentation mechanism in diamond (111) crystals.[21,25]

In this work, a (1×1) hydrogen-terminated diamond (111) surface is brought into sliding contact with another (1×1) hydrogen-terminated diamond (111) surface. The carbon portion of a diamond (111) surface consists of first- and second-layer carbon atoms that are trigonally arranged. The vertices of these triangles are rotated 60° with respect to one another, thus forming a hexagon. (It is important to note that this hexagon is not planar but, rather, more similar to the chair conformation in cyclohexane.) These hexagons are centered over the fourth-layer carbon atoms, which are visible through "windows" or "holes" in the surface layer. The hydrogen atoms that cover the diamond surface are bound to the first-layer carbon atoms.

The lattices contain ten layers of carbon atoms and two layers of hydrogen atoms, where each layer contains 16 atoms [Fig. 1(a)]. Periodic boundary conditions are applied in the XY plane that contains the (111) surface of the lattices. This simulates an infinite (111) sliding interface. The atoms of the three outermost layers (in the Z

and $-Z$ direction) of each lattice are held rigid. Frictional forces[26] are applied to the atoms of the next five layers of both the upper and the lower lattice to control the temperature of the system. The atoms of the four innermost layers of each lattice have no constraints placed on them.

Sliding is performed by moving the rigid layers of the upper lattice at a constant velocity over the lower lattice while maintaining a constant separation between the rigid layers. It should be noted that, in a typical experiment, the load rather than the distance is normally held constant. The principal effect of the load is to vary the contact area in the presence of surface roughness; since these surfaces are atomically flat, this effect is not relevant.[17] The values of sliding velocity v examined here are 0.5 Å/ps (50 m/s) and 1.0 Å/ps (100 m/s). The normal force and the frictional force on each lattice is calculated by summing the forces on each rigid-layer atom and averaging this sum over 20 time steps. These forces are then divided by the number of atoms in the rigid layer to obtain the force per atom. The positions and velocities of each atom are recorded at various equally spaced time intervals throughout the simulation. These data are then used to construct a video animation sequence of the sliding experiment. These molecular-dynamics "movies" proved invaluable in the analysis of the sliding process and the elucidation of the sliding mechanism.

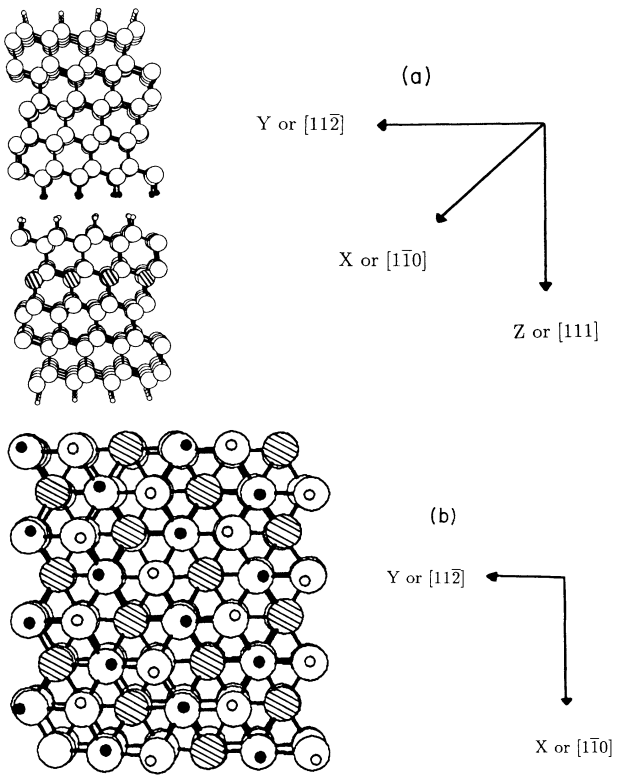

FIG. 1. (a) Initial configurations for the diamond (111) surfaces examined here viewed along the [$\bar{1}$10] direction. In this view, large open circles represent carbon atoms, small open circles represent hydrogen atoms of the lower surface, cross-hatched atoms represent fourth-layer carbon atoms of the lower surface, and small filled circles represent hydrogen atoms from the upper surface. (b) Only the lower surface and hydrogen atoms of the upper surface are shown, viewed along the [111] direction. Large open circles represent carbon atoms of the lower surface, small open circles, cross-hatched atoms, and small filled circles are the same as in (a).

III. RESULTS

Initial atomic configurations for the hydrogen-terminated (111) lattices are shown in Fig. 1. The layer structure of these systems is evident in the side view ([$\bar{1}$10] direction) shown in Fig. 1(a). To show the placement of hydrogen atoms of the upper surface relative to the lower surface, the (111) surface view has also been included in Fig. 1(b). In this view, only the hydrogen atoms of the upper surface and the lower-lattice atoms are shown. These atoms are viewed along the [111] direction. The large circles are carbon atoms in the lower surface, cross-hatched circles are fourth-layer carbon atoms of the lower surface, small open circles are terminal hydrogen atoms of the lower crystal, and small filled circles are terminal hydrogen atoms of the upper surface. This perspective will be subsequently referred to as the "surface view."

Figure 1(b) shows one of the starting configurations examined here. In this case, the hydrogen atoms of the upper surface are centered over second-layer carbon atoms of the lower surface. The hydrogen atoms of the two surfaces are lined up in the [11$\bar{2}$] (or Y) sliding direction (but not in the [1$\bar{1}$0] (or X) sliding direction).

We have examined friction as a function of crystallographic sliding direction, sliding velocity, normal load, temperature, and starting configuration. The normal load on the lattices is increased by bringing the rigid layers of both lattices closer together. The friction coefficient μ is defined as the average frictional force, divided by the average normal force, e.g., $\langle F_y \rangle / \langle F_z \rangle$. The average normal pressure $\langle P_z \rangle$ is defined as $\langle F_z \rangle$ divided by the area of the rigid layer in the XY plane. The surface separation is defined as the Z distance between the hydrogen atom layer on the upper surface and the hydrogen atom layer on the lower surface. The Z distance of a hydrogen atom layer is defined as the average Z position of all the hydrogen atoms in the layer.

A. Load dependence

1. Sliding in the [11$\bar{2}$] direction

With the surfaces configured as in Fig. 1(b), the upper surface is slid in the [11$\bar{2}$] direction at 1.0 Å/ps with the temperature of the system maintained at 300 K. The force normal to the sliding interface, F_z, and the force parallel to the sliding direction, F_y, i.e., the shear force, on the rigid layers of the upper surface are shown as a function of distance (in units of unit-cell length) in Fig. 2(a). (To determine the normal loading force, for example, simply multiply F_z by the total number of atoms in the rigid layers of the upper surface.) In this direction, the repeat distance is 4.357 Å, the distance between surface hydrogen atoms in the [11$\bar{2}$] direction. The average

normal pressure $\langle P_z \rangle$ on the upper lattice over the entire simulation is 1.9 GPa and the friction coefficient μ is 0.037. The F_z curve is periodic, exhibiting one symmetric maximum per unit cell. In contrast, the F_y data are also periodic with one maximum per unit cell; however, these maxima are not symmetric. It is also important to note that the maxima in the F_y data consistently occur before the maxima in the F_z data.

In an effort to gain insight into the shapes of the peaks in the F_y and F_z data, the periodic structure of these data, and the displacement of the F_y maxima with respect to the F_z maxima, the atomistic mechanism of the sliding process has been examined. As the upper lattice slides over the lower lattice in the $[11\bar{2}]$ direction, the terminal hydrogen atoms of the upper surface pass over the second-layer carbon atoms, then over fourth-layer carbon atoms of the lower lattice before encountering the hydrogen atoms on the lower surface. As the hydrogen atoms of the upper sliding surface begin to interact repulsively with the hydrogen atoms on the lower surface, both F_z and F_y increase. If the hydrogen atoms of both surfaces were held rigid, the hydrogen atoms of the upper surface would be forced to pass directly over the hydrogen atoms of the lower surface. However, since the system has some thermal motion and the repulsive interaction is relatively strong, the hydrogen atoms are able to "revolve" around one another in the XY plane. That is, each hydrogen atom of the upper surface follows a half-circle path about the hydrogen atom on the lower surface closest to it. This motion reduces some of the shear force in the $[11\bar{2}]$ direction; thus, F_y begins to decrease. Once the hydrogen atoms of the upper surface have revolved around the hydrogen atoms on the lower surface, the hydrogen-hydrogen repulsive interaction *pushes* the upper-surface hydrogen atoms in the sliding direction. This corresponds to the negative portion of the peak in the F_y data shown in Fig. 2(a). The flat part of this curve corresponds to a region where the hydrogen atoms of both surfaces are only weakly interacting. The maxima in the frictional force data occur just prior to the revolution of the hydrogen atoms. This motion of the hydrogen atoms has little effect on the force normal to the sliding direc-

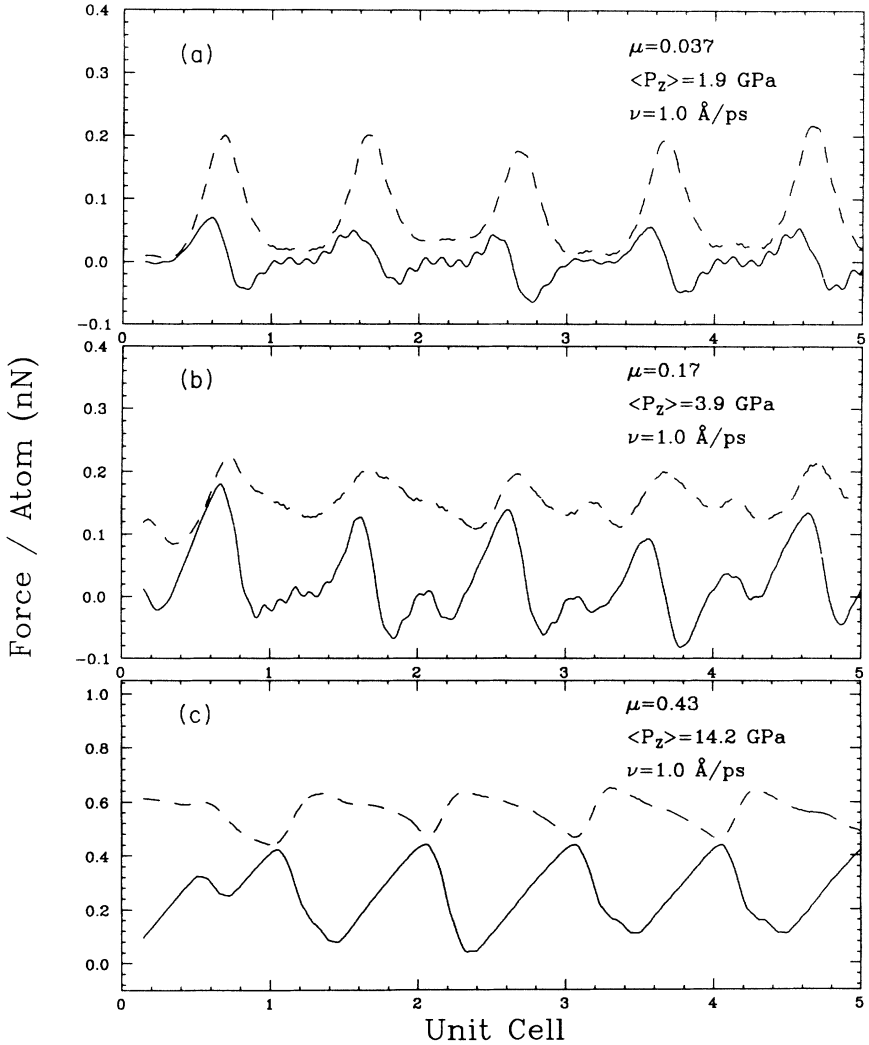

FIG. 2. Frictional force and normal force per atom as a function of unit cell length for sliding the rigid layers of the upper surface in the $[11\bar{2}]$ direction at 1.0 Å/ps and 300 K for three different values of applied load. Dashed lines represent F_z and solid lines represent F_y. [Starting configurations are as in Fig. 1(b).]

tion. The maxima in the F_z data occur when the hydrogen atoms of the upper surface pass over (albeit not directly) the hydrogen atoms of the lower surface. Thus, F_y has already begun to decrease when F_z is at a maximum. The F_z maximum corresponds to the point of maximum hydrogen-hydrogen repulsive interaction. This is evident from a plot of the separation between the upper and lower surfaces versus sliding distance [Fig. 3(a)]. These data are periodic, with one symmetric peak per unit cell. The positions of these maxima correspond exactly with the positions of the maxima in the F_z data [Fig. 2(a)]. The increased repulsive interaction between the hydrogen atoms causes an increase in the separation between the two surfaces. Similarly, the minima in the surface separation occur at the same points as the minima in the F_z data.

Increasing the load on the lattices and sliding the rigid layer of the upper lattice in the $[11\bar{2}]$ direction at 1.0 Å/ps (while maintaining the temperature at 300 K) yields the F_z and F_y data shown in Fig. 2(b). For these data $\langle P_z \rangle = 3.9$ GPa and $\mu = 0.17$. The atomistic sliding mechanism at this load is qualitatively similar to the lower-load mechanism discussed earlier. In this case, analysis of the video animation sequence reveals that the revolution of the hydrogen atoms about one another to reduce repulsion is more pronounced, i.e., the hydrogen atoms are pushed farther away from one another in the plane of the surface. Also, the surface separation versus distance data mirrors the F_z data as before; however, in this case the change in separation is less [Fig. 3(b)]. This is not surprising in light of the increased pressure. In this case, both the F_z and the F_y data contain two maxima per unit cell, one larger peak, followed by a smaller peak, both of which are approximately symmetric. The larger peaks in both sets of data correspond to the same type of hydrogen-hydrogen repulsive interaction described for the low-load data [Fig. 2(a)]. The smaller peaks arise from hydrogen-carbon repulsive interactions. For example, after the surface hydrogen atoms of the upper lattice slide over the terminal hydrogen atoms of the lower surface they encounter second-layer carbon atoms of the lower surface [see Fig. 1(b)]. Due to the closer proximity of the surfaces at this load, this repulsive interaction results in the smaller peaks in the data shown in Fig. 2(b).

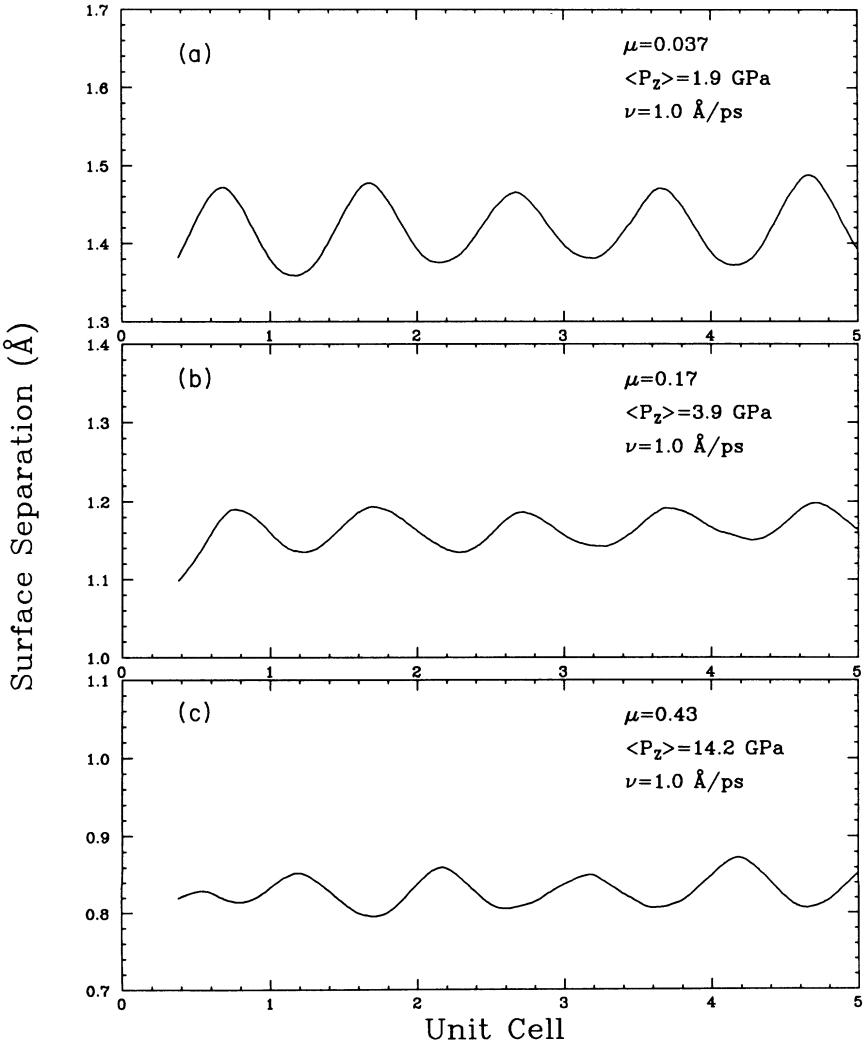

FIG. 3. Surface separation as a function of unit-cell length for the simulations shown in Fig. 2.

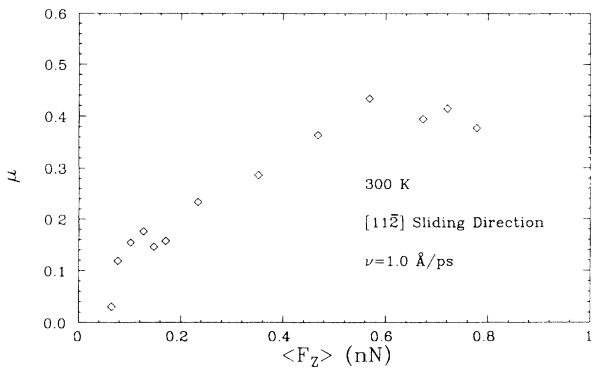

FIG. 4. Friction coefficient as a function of load for sliding in the [11$\bar{2}$] direction at 1.0 Å/ps and 300 K.

Further increasing the load and repeating the simulation with the same conditions used earlier (300 K and $v=1.0$ Å/ps) yields different behavior. For this simulation $\langle P_z \rangle = 14.2$ GPa and $\mu = 0.43$. In this case, F_y [see Fig. 2(c)] is still periodic with one broad maximum per unit cell; however, the larger peak is now asymmetric. That is, the magnitude of the slope for the ascending portion of this peak is less than for the descending (latter) portion. This type of behavior is known as stick-slip.[9,10] The frictional force increases linearly with unit-cell distance as the in-plane hydrogen-hydrogen repulsive interaction increases. Due to the increased load, the hydrogen atoms are momentarily "stuck" in the head-on alignment. The frictional force builds up until the hydrogen atoms can revolve around one another, resulting in a "slip," concomitant with a large decrease in F_y. The video animation sequence supports this interpretation. The "slip" causes the hydrogen atoms of the upper surface to pass over the second-layer carbon atoms of the lower surface very quickly. As a result, the smaller maxima visible in the 3.9-GPa data are no longer resolved. (The slope of the desending portion of the peak changes slightly near the baseline hinting at the presence of the unresolved smaller peak.) The F_z data also exhibit one very broad maximum per unit cell. Similar to the F_y data, the very close proximity of the two lattices at this load has caused the broadening of the two previously observed maxima (3.9 GPa) such that the smaller peak is not resolved. This broadening is also evident in the surface separation data shown in Fig. 3(c). Finally, the maxima in the F_z data are displaced further from the F_y maxima at this load than at the lower loads. This is again due to the stick-slip behavior observed at this load.

Analysis of the three previous simulations suggests that as load is increased μ also increases. This behavior is illustrated in Fig 4. Here μ increases with increasing load until the load is approximately 0.6 nN. In this region, as the load is increased the repulsive interaction between the surfaces increases. As a result it becomes more difficult for the hydrogen atoms of the upper surface to pass over the lower surface, increasing $\langle F_y \rangle$. For loads higher than 0.6 nN, increasing the load is not concomitant with an increase in $\langle F_y \rangle$, but rather with compression of the bulk lattice. Therefore, since $\langle F_z \rangle$ increases significantly but $\langle F_y \rangle$ does not, μ decreases slightly.

It should be noted that shifting the upper lattice in the [11$\bar{2}$] direction and repeating the simulations discussed above merely shifts the location of the maxima in F_z and F_y. It does not alter the atomistic sliding mechanism, μ, or $\langle P_z \rangle$ significantly.

2. *Sliding in the [1$\bar{1}$0] direction*

Beginning with the same initial positions [Fig. 1(b)] but now sliding the upper lattice in the [1$\bar{1}$0] direction at 1.0 Å/ps and 300 K yields the F_z and frictional-force F_x data shown in Fig. 5(a). For this simulation $\mu = 0.001$ and $\langle P_z \rangle = 0.98$ GPa. (The distance between the hydrogen atoms in this direction is 2.524 Å.) These data are similar to the data obtained from the [11$\bar{2}$] slide (at a similar pressure) in that they are periodic in distance; however, they differ in some respects. For example, the maxima in the F_z and F_x data are broader than for sliding in the [11$\bar{2}$] direction [Fig. 2(a)]. Additionally, the maxima in the F_x data are now symmetric, oscillating about zero, and contain no flat regions. This is due to the much smaller distance between surface hydrogen atoms and to the different sliding mechanism when sliding in this direction. The oscillations about zero in the F_x data give rise recall that to very small $\langle F_x \rangle$ and as a result μ is very small.

At the start of the simulation the surface hydrogen atoms of the upper surface are over second-layer carbon atoms of the lower surface. As the rigid layers of the upper surface slide in the [1$\bar{1}$0] direction these hydrogen atoms begin to interact with hydrogen atoms on the lower surface. This is accompanied by an increase in F_z and F_x. But now, instead of being in the head-on alignment, the hydrogen atoms of the upper surface are initially located at a diagonal to the hydrogen atoms of the lower surface. Thus, when the hydrogen atoms of opposite surfaces begin to interact, the hydrogen atoms of the upper surface are gradually displaced in the direction toward fourth-layer carbon atoms of the lower surface [see Fig. 1(b)]. That is, as the surface hydrogen atoms come into closer proximity the repulsive interaction "pushes" these hydrogen atoms farther apart in the XY plane. This motion relieves stress in the [1$\bar{1}$0] direction, reducing F_x, and begins to increase stress in the [11$\bar{2}$] direction. The configuration just prior to the point where stress is relieved in the [1$\bar{1}$0] direction corresponds to a maximum in the F_x data. The point when the hydrogen atoms of the sliding surface are approximately over fourth-layer lower-surface carbon atoms corresponds to a maximum in the F_z data and to a maximum in the stress in the [11$\bar{2}$] direction [see Fig. 5(a)]. This also corresponds to the point of maximum surface separation [Fig. 6(a)]. Continued sliding in the [1$\bar{1}$0] direction allows the hydrogen atoms to move back to positions over second-layer carbon atoms. This configuration results in a minimum in both the F_z [Fig. 5(a)] and the surface separation data [Fig. 6(a)]. The net result is the surface hydrogen atoms of the upper surface appear to "zigzag" over the lower surface.

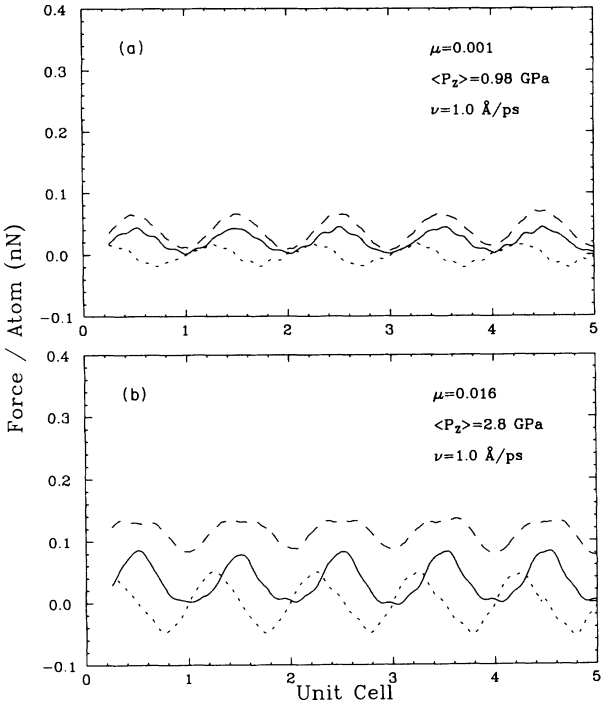

FIG. 5. Frictional force and normal force per atom as a function of unit-cell length for sliding the rigid layers of the upper surface in the $[1\bar{1}0]$ direction at 1.0 Å/ps and 300 K for two different values of applied load. Dashed lines represent F_z, solid lines represent F_y, and dotted lines represent F_x. [Starting configurations are as in Fig. 1(b)].

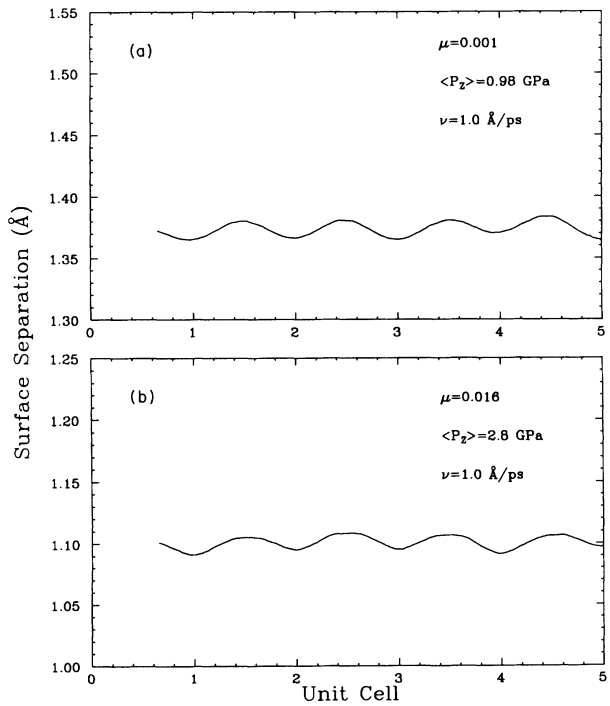

FIG. 6. Surface separation as a function of unit-cell length for the simulations shown in Fig. 5.

Increasing the load on the lattices and repeating the sliding in the $[1\bar{1}0]$ direction yields the F_z and F_x data shown in Fig. 5(b). The friction coefficient is 0.01 and $\langle P_z \rangle = 2.8$ GPa. Both sets of data are periodic, with one maximum per unit cell. In contrast to the low-load slide, here the F_z data are asymmetric. The sliding mechanism is very similar to the low-load $[1\bar{1}0]$ sliding case. That is, the hydrogen atoms of the upper surface still appear to zigzag over the lower surface. However, at this pressure the zigzag motion is more pronounced, i.e., the hydrogen atoms are pushed farther apart, which results in an increased stress in the $[11\bar{2}]$ direction [see Fig. 5(b)]. The maxima in the F_z data correspond to maxima in the surface separation data as in the low-load case [Fig. 6(b)].

The asymmetry of the F_z peak is explained as follows. Consider one peak; the increasing portion of this peak corresponds to the movement of the upper-surface hydrogen atoms to a position approximately over the holes in the lower surface. To complete the slide these hydrogen atoms must move diagonally back to a position over the second-layer carbon atoms. At higher pressure, the two lattices are closer together which increases the interaction between surface hydrogen atoms and second-layer carbon atoms of the opposite surface. This interaction opposes the movement of these hydrogen atoms out of the holes, thereby accounting for the asymmetry of the peaks in the F_z data. In other words, at this pressure it takes more effort to climb out of the hole than to fall in.

Due to the differing sliding mechanism when sliding in the $[1\bar{1}0]$ direction versus the $[11\bar{2}]$ direction, increasing the load does not increase μ as much as it does for sliding in the $[\bar{1}1\bar{2}]$ direction. Increasing the load increases the magnitude of the oscillations of F_x about zero; however $\langle F_x \rangle$ is still fairly small. Thus, μ is only slightly different at higher loads.

B. Directional dependence

For the initial configuration shown in Fig. 1(b) and approximately the same value of $\langle F_z \rangle$, the friction coefficients tend to be an order of magnitude smaller when sliding in the $[1\bar{1}0]$ direction versus sliding in the $[11\bar{2}]$ direction. This is attributed to the different sliding mechanisms. In the $[11\bar{2}]$ direction, the hydrogen atoms of the upper and lower surfaces are aligned. Therefore, when sliding in this direction the terminal hydrogen atoms of both surfaces come into direct contact and as a result must revolve around one another. This head-on repulsive interaction increases the friction coefficient. In the $[1\bar{1}0]$ direction, the hydrogen atoms zigzag from positions over second-layer carbon atoms to positions over holes of the lower surface. This mechanism does not allow for head-on hydrogen-hydrogen interaction; thus, the friction coefficients are lower for sliding in this direction.

Due to the close proximity of the hydrogen atoms in the $[1\bar{1}0]$ direction it is difficult to get the hydrogen atoms of the upper and lower surface aligned in this direction. The hydrogen atoms make space for themselves by pushing hydrogen atoms on the opposite surface, which are in close proximity, away from them in either the $[11\bar{2}]$ or the $[\bar{1}\,\bar{1}2]$ direction. Therefore, for slid-

ing in the [1$\bar{1}$0] direction the vast majority of simulations exhibit the zigzag motion described previously.

C. Sliding-velocity dependence

1. Sliding in the [11$\bar{2}$] direction

Reducing the sliding speed to 0.5 Å/ps and repeating the low- and high-load simulations at 300 K yields the F_z and F_y data as a function of distance shown in Fig. 7. Comparison of Fig. 7(a) with Fig. 2(a) and Fig. 7(b) with Fig. 2(c) reveals that these data are qualitatively very similar. For the low-load 0.5-Å/ps simulations, the magnitudes of the maxima in the F_z and the F_y data are slightly larger than for the 1.0-Å/ps simulation. The slower sliding velocity allows the hydrogen atoms of the upper and lower surfaces to remain aligned head on in the [11$\bar{2}$] sliding direction longer before the revolution of the hydrogen atoms about one another to relieve stress. This causes the slight increase in the maxima of both the F_z and the F_y data. Since the hydrogen atoms are closer together after the rotation, the hydrogen atoms of the lower surface can give the hydrogen atoms of the upper surface a slightly larger push in the sliding direction. As a result, the slope of the F_y data between a maximum and a minimum (in the sliding direction) is slightly larger than for the 1.0-Å/ps data.

Similarly, for the high-load 0.5-Å/ps slide [Fig. 7(b)] the terminal hydrogen atoms of both surfaces remain in the head-on configuration (or stuck) longer than for the 1.0-Å/ps slide [Fig. 2(c)]. This results in slightly larger maxima in both the F_z and F_y data and for a more pronounced slip. At this slower sliding velocity, the smaller peak which is due to the interaction of the upper-surface hydrogen atoms with the second-layer carbon atoms of the lower surface is sometimes resolved.

These differences in the 0.5-Å/ps data versus the 1.0-Å/ps sliding data are small and do not significantly alter the sliding mechanism, μ, or $\langle P_z \rangle$. Therefore, for the sliding velocities examined here, the friction phenomenon in the [11$\bar{2}$] direction is not dependent on the sliding velocity to a great extent. (However, these results do hint that for sliding velocities much lower than those examined here the differences may be more pronounced.) At present, we cannot comment on the dependence on slower sliding velocities more closely approximating experimental sliding speeds, since computational constraints prevent the examination of sliding velocities orders of magnitude slower than 0.5 Å/ps. (In order to achieve very slow computational sliding speeds, a highly parallel version of this code is currently under construction.)

The frictional forces cannot draw heat away from sliding interface quickly enough to maintain the temperature of the system for sliding velocities faster than 1.0 Å/ps. This is not a concern since experimental sliding speeds tend to be orders of magnitude slower.

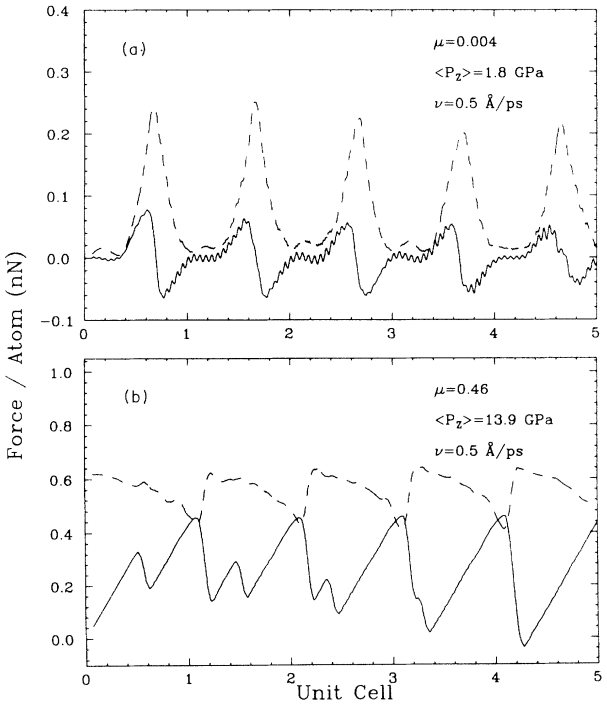

FIG. 7. For two values of applied load, frictional force, and normal force per atom as a function of unit-cell length for sliding the rigid layers of the upper surface in the [11$\bar{2}$] direction at 0.5 Å/ps and 300 K. Dashed lines represent F_z and solid lines represent F_y. [Starting configurations are as in Fig. 1(b).]

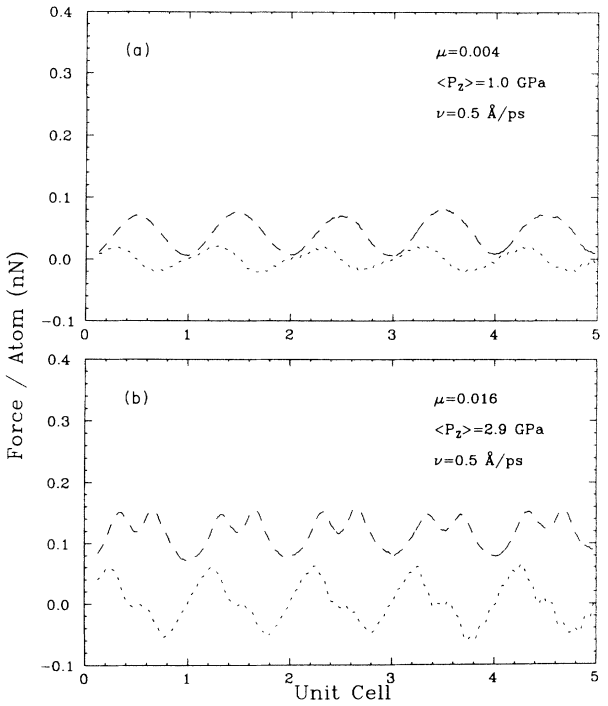

FIG. 8. For two values of applied load, frictional force, and normal force per atom as a function of unit-cell length for sliding the rigid layers of the upper surface in the [1$\bar{1}$0] direction at 0.5 Å/ps and 300 K. Dashed lines represent F_z and dotted lines represent F_x. [Starting configurations are as in Fig. 1(b).]

2. *Sliding in the [1$\bar{1}$0] direction*

Reducing the sliding velocity to 0.5 Å/ps and repeating both the low- and high-load simulations yield the F_z and the F_x shown in Fig. 8. At low load, these data are virtually identical to these same data obtained from the 1.0-Å/ps sliding simulation [Fig. 5(a)]. At higher loads, however, the shapes of the F_z and F_x data are different [Fig. 8(b)] from the faster sliding velocity. In this case, in both the F_z and F_x data the maxima have developed structure. That is, the F_z maxima have split into two peaks and similarly, the F_x maxima have developed a shoulder on the descending portion of the peak. While there are hints of these features in these same data at the faster sliding velocity [Fig. 5(b)] they are much more pronounced at this sliding velocity.

As described earlier, when the hydrogen atoms of the upper surface begin to move in the [1$\bar{1}$0] direction, they begin to interact with the hydrogen atoms of the lower surface. This increases F_x. As a result of this interaction, the hydrogen atoms of both surfaces are pushed away from one another in the XY plane, increasing the stress in the [11$\bar{2}$] direction and decreasing F_x slightly. This results in the formation of the first small peak in F_z.

These differences in the shapes of the F_z and F_x data do not alter μ significantly; however, this added structure does yield more insight into the sliding mechanism, although it is basically unchanged. Therefore, for sliding directions where the head-on arrangement of surface atoms is not encountered, the sliding velocity may not be as important as it is when head-on alignments of atoms are encountered.

D. Temperature dependence

The friction coefficient μ is shown as a function of temperature in Fig. 9. These data were well generated by starting with the initial configuration shown in Fig. 1(b) and sliding in the [11$\bar{2}$] direction for a total of 15.0 ps while the temperature of the system was maintained at the desired value. Due to differences in the degree of thermal motion at different temperatures, $\langle P_z \rangle$ for these simulations varies from 2.7 GPa for the 10 K run to 3.6 GPa at 300 K.

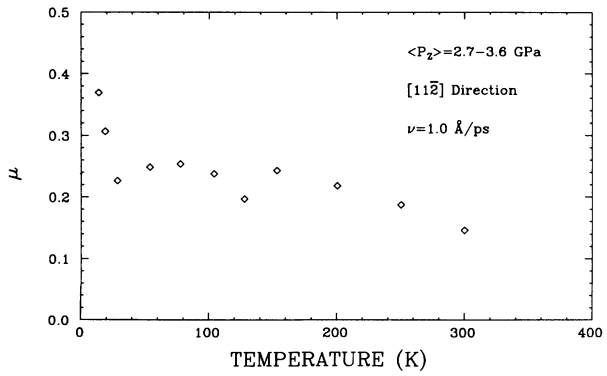

FIG. 9. Friction coefficient as a function of temperature for sliding in the [11$\bar{2}$] direction at 1.0 Å/ps and 300 K. [Starting configurations are as in Fig. 1(b).]

The friction coefficient is greatest at 10 K, dropping sharply from 10 to 50 K. From 50 to 150 K, μ is approximately constant and from 150 to 300 K, μ decreases as the temperature increases. This behavior is easily explained in light of the sliding mechanism. As noted earlier, for the hydrogen atoms of the upper surface to slide past the hydrogen atoms on the lower surface they must first be pushed away from each other in the XY plane so that they can revolve about one another. At higher temperatures (150–300 K) the increased amount of thermal motion aids this process; as a result, μ is lower. At very low temperatures (10 K) where the thermal motion is negligible, this "revolution" of hydrogen atoms becomes very difficult; thus, μ is greater.

IV. DISCUSSION

Macroscopic friction is usually accompanied by wear and energy is dissipated in the bulk material by the movement of dislocations. In contrast, at the atomic level, recent experiments[9,10] have shown that friction may not always be accompanied by wear.

Various simple models[15,16] have been invoked to reveal the basic principles of this so-called "wearless friction." Two of these simple models, the independent oscillator model[15] (IO) and the Frenkel-Kontorova Model,[16] have been shown to predict the same qualitative trends.[17]

The essence of the IO model is summarized below. Consider two atomically flat solids, A and B, sliding over one another. At the sliding interface, the B solid has surface atoms (denoted as B_0) attached to it by harmonic springs. These atoms can lose energy to the support through vibration. As the surfaces slide over one another, any given B_0 atom experiences the potential V_{AB} arising from the interaction of the two surfaces. It is the shape of V_{AB} which ultimately governs the friction process. For example, for strongly interacting surfaces V_{AB} will contain various local extrema. A given B_0 atom passes through various metastable local minima upon sliding. Falling from these metastable minima to a lower minimum causes B_0 to become vibrationally excited, a process termed "plucking." This vibrational energy is then dissipated to the solid as heat. Thus, plucking results in strain energy of translation being converted to vibrational energy which is the essence of the atomic-scale friction process. For very weakly interacting solids the friction vanishes, since V_{AB} would contain no metastable local minima. The directional dependence of friction is implicit in this model. A different placement of atoms implies a different interaction potential V_{AB} governing the friction process.

The simulations presented here contain a larger degree of information than one could obtain from the earlier models of wearless friction. However, it is interesting to note that the predictions derived from these simple models are consistent with the findings presented here. For example, the directional dependence of friction is implicit in this model. A different placement of atoms implies a different interaction potential V_{AB} governing the friction process. In our system, different atom placements are en-

countered when sliding in the $[1\bar{1}0]$ direction of a diamond (111) surface versus the $[11\bar{2}]$ direction. Therefore, these simple models would predict that the friction should be different in these two directions; a prediction which is borne out by these more sophisticated MD simulations. The shape of the frictional force versus distance functions [Figs. 2(a) and 5(a)] are very different when sliding in these two directions for approximately the same $\langle P_z \rangle$ and temperature. Ultimately, this results in a lower μ for sliding in the $[1\bar{1}0]$ direction.

On the macroscopic scale, the frictional properties of various single crystals have been measured, and it has been shown that the frictional forces of some crystals are anisotropic with respect to the crystallographic direction of sliding.[1,4,27,28] Additionally, there have been several studies of the effect of load on the friction coefficients of diamond sliding on diamond. However, some investigators found it increases with load,[4] some found it is independent of load,[2] and recently, it has been reported that different dependencies on load are obtained for different crystal and polish orientations.[7,29] It is difficult to compare these traditional friction measurements to atomic-scale measurements because the experimental measurements are averaged over large heterogeneous samples. However, it is interesting to note that we also observe frictional anisotropy in our atomic-scale simulations.

While these simulations agree qualitatively with the simple model discussed earlier, they also provide additional insight into the friction process. For example, the mechanism of the sliding process was investigated at the atomic scale. It was determined that this mechanism differs depending upon sliding direction. Additionally, it was determined that the frictional behavior is independent of sliding velocity at 300 K. Finally, the explicit dependence of μ on applied load and temperature was elucidated. Subsequent publications will investigate the role of surface defects (e.g., radical sites) and the role of adsorbed species (e.g., CH_3) in the friction process, all of which are not addressed by simple models such as the IO model.

ACKNOWLEDGMENTS

This work was partially supported by the Office of Naval Research under Contract No. N00014-92-WX-24183. J.A.H. acknowledges support from the Office of Naval Technology. J.A.H. would also like to thank Dr. Gary M. McClelland for many helpful discussions.

*Author to whom correspondence should be addressed.

[1]F. P. Bowden and C. A. Brookes, Proc. R. Soc. London Ser. A **295**, 244 (1966).
[2]M. Casey and J. Wilks, J. Phys. D **6**, 1772 (1973).
[3]D. Tabor, in *Properties of Diamond,* edited by J. E. Field (Academic, London, 1979), pp. 325–350.
[4]Y. Enomoto and D. Tabor, Proc. R. Soc. London Ser. A **373**, 405 (1981).
[5]M. Seal, Philos. Mag. A **43**, 587 (1981).
[6]B. Samuels and J. Wilks, J. Mater. Sci. **23**, 2846 (1988).
[7]I. P. Hayward, Surf. Coat. Technol. **49**, 554 (1991).
[8]F. P. Bowden and D. Tabor, *The Friction and Lubrication of Solids* (Oxford, Clarendon, 1964), Vol. 2.
[9]C. M. Mate, G. M. McClelland, R. Erlandsson, and S. Chiang, Phys. Rev. Lett. **59**, 1942 (1987).
[10]R. Erlandsson, G. Hadziloannou, C. M. Mate, G. M. McClelland, and S. Chiang, J. Chem. Phys. **89**, 5190 (1988).
[11]P. A. Thompson and M. O. Robbins, Phys. Rev. Lett. **63**, 766 (1989).
[12]W. Zhong and D. Tomanek, Phys. Rev. Lett. **64**, 3054 (1990).
[13]J. B. Sokoloff, Phys. Rev. B **42**, 760 (1990).
[14]U. Landman and W. D. Luedtke, J. Vac. Sci. Tech. B **9**, 414 (1991).
[15]G. A. Tomlinson, Philos. Mag. **7**, 905 (1929).
[16]F. C. Frenkel and T. Kontorova, Zh. Eksp. Teor. Fiz. **8**, 1340 (1938).
[17]G. M. McClelland and J. N. Glosli, in *NATO Advanced Study Institute Proceedings on Fundamentals of Friction: Macroscopic and Microscopic Processes,* edited by I. L. Singer and H. M. Pollock (Kluwer, Dordrect, 1992), pp. 405–426.
[18]J. B. Sokoloff, Surf. Sci. **144**, 267 (1984).
[19]M. Hirano and K. Shinjo, Phys. Rev. B **41**, 11 837 (1984).
[20]C. W. Gear, *Numerical Initial Value Problems in Ordinary Differential Equations* (Prentice-Hall, Englewood Cliffs, NJ, 1971).
[21]J. A. Harrison, D. W. Brenner, C. T. White, and R. J. Colton, Thin Solid Films **206**, 213 (1991).
[22]D. W. Brenner, Phys. Rev. B **42**, 9458 (1990).
[23]D. W. Brenner, J. A. Harrison, C. T. White, and R. J. Colton, Thin Solid Films **206**, 220 (1991).
[24]R. C. Mowrey, D. W. Brenner, B. I. Dunlap, J. W. Mintmire, and C. T. White, J. Phys. Chem. **95**, 7138 (1991).
[25]J. A. Harrison, C. T. White, R. J. Colton, and D. W. Brenner, Surf. Sci. **271**, 57 (1992).
[26]H. J. C. Berendsen, J. P. M. Postma, W. F. van Gunsteren, A. DiNola, and J. R. Haak, J. Chem. Phys. **81**, 3684 (1984).
[27]D. H. Buckley and K. Miyoshi, in *Structural Ceramics,* edited by J. B. Watchman, Jr. (Academic, San Diego, 1989), Vol. 29, p. 300.
[28]M. Hirano, K. Shinjo, R. Kaneko, and Y. Murata, Phys. Rev. Lett. **67**, 2642 (1991).
[29]B. Samuels and J. Wilks (unpublished).